THE JOURNAL OF BIOLOGICAL CHEMISTRY VOL. 284, NO. 30, pp. 20299–20310, July 24, 2009

The Role of Carbonic Anhydrase 9 in Regulating Extracellular and Intracellular pH in Three-dimensional Tumor Cell Growths*[S]

Received for publication, April 9, 2009 Published, JBC Papers in Press, May 19, 2009, DOI 10.1074/jbc.M109.006478

Pawel Swietach[‡], Shalini Patiar[§], Claudiu T. Supuran[¶], Adrian L. Harris[§1], and Richard D. Vaughan-Jones[‡1,2]

From the [‡]Department of Physiology, Anatomy and Genetics, Burdon Sanderson Cardiac Science Centre, Oxford OX1 3PT, United Kingdom, the [§]Weatherall Institute of Molecular Medicine, Oxford OX3 9DS, United Kingdom, and the [¶]Laboratorio di Chimica Bioinorganica, Universita degli Studi di Firenze, I-50019 Firenze, Italy

We have studied the role of carbonic anhydrase 9 (CA9), a cancer-associated extracellular isoform of the enzyme carbonic anhydrase in multicellular spheroid growths (radius of ~300 μm) of human colon carcinoma HCT116 cells. Spheroids were transfected with CA9 (or empty vector) and imaged confocally (using fluorescent dyes) for both intracellular pH (pH_i) and pH in the restricted extracellular spaces (pH_e). With no CA9 expression, spheroids developed very low pH_i (~6.3) and reduced pH_e (~6.9) at their core, associated with a diminishing gradient of acidity extending out to the periphery. With CA9 expression, core intracellular acidity was less prominent (pH_i = ~6.6), whereas extracellular acidity was enhanced (pH_e = ~6.6), so that radial pH_i gradients were smaller and radial pH_e gradients were larger. These effects were reversed by eliminating CA9 activity with membrane-impermeant CA inhibitors. The observation that CA9 activity reversibly reduces pH_e indicates the enzyme is facilitating CO_2 excretion from cells (by converting vented CO_2 to extracellular H^+), rather than facilitating membrane H^+ transport (such as H^+ associated with metabolically generated lactic acid). This latter process requires titration of exported H^+ ions with extracellular HCO_3^-, which would reduce rather than increase extracellular acidity. In a multicellular structure, the net effect of CA9 on pH_e will depend on the cellular CO_2/lactic acid emission ratio (set by local oxygenation and membrane HCO_3^- uptake). Our results suggest that CO_2-producing tumors may express CA9 to facilitate CO_2 excretion, thus raising pH_i and reducing pH_e, which promotes tumor proliferation and survival. The results suggest a possible basis for attenuating tumor development through inhibiting CA9 activity.

The carbonic anhydrases (CAs)[3] are a family of enzymes that reversibly catalyze CO_2 hydration to H^+ and HCO_3^- (1, 2). Recent studies have identified several CA isoforms, such as CA4, CA9, CA12, and CA14, with extracellular-facing catalytic sites (2). Many cells express extracellular CA (CA_e) isoforms, but their physiological role remains unclear. In particular, the strong link between cancer and CA9 expression (1–5) has provoked great interest in the role of CA_e in tumor biology.

Based on their topology, CA_e isoforms are likely to regulate the concentration of extracellular H^+, CO_2, and HCO_3^-. Cell metabolism drives transmembrane fluxes of H^+ ions, CO_2 and HCO_3^-, and can provide substrate for the CA_e-assisted reaction. For example, CO_2 is released from aerobically respiring cells. By consuming or producing H^+ ions, the CA_e-catalyzed reaction will affect extracellular pH (pH_e). Many membrane proteins are modulated by pH_e (6–8). Some of these are acid/base transporters that regulate intracellular pH (pH_i) (9). Such modulation allows pH_e to cross-talk with pH_i (10, 11), thus helping to shape the plethora of effects that pH_i has on cellular physiology (3, 9, 12, 13). Extracellular pH can also affect tissue structure through the release or modulation of proteolytic enzymes that act on the extracellular matrix (14, 15). In addition, the pH_e-pH_i difference is important in determining the distribution of membrane-permeant weak acids/bases, which include many drugs used clinically (*e.g.* doxorubicin).

A complete understanding of pH regulation at tissue level requires characterization of events occurring within cells, at their surface membrane, and in the surrounding extracellular space. To date, many pH studies have treated the extracellular space as an infinite, well-stirred, and equilibrated compartment of constant pH. This condition is compatible with experimentally superfused, isolated cells, but it may not apply to all cells *in situ*. Blood plasma is a major component of extracellular fluid. In health, plasma pH is regulated to ~7.4 by the lungs and kidneys, acting in concert to remove excess acid/base that has been added to blood from dietary or cellular sources. Tissue fluid occupies the gap between plasma and cells (with the exception of blood-borne cells). Under conditions of ideal diffusive coupling between cells and capillaries, pH_e in tissue fluid would be held close to plasma pH. However, pH_e close to the cell surface can diverge from 7.4, particularly when the cell-capillary distance is increased (*e.g.* as a result of poor blood

* This work was supported by funds from the Royal Society and Medical Research Council (to P. S.), the British Heart Foundation and Wellcome Trust (to R. D. V.-J.), EUROXY, and Cancer Research UK (to A. L. H.).

[S] The on-line version of this article (available at http://www.jbc.org) contains supplemental Figs. S1–S4 and details of the mathematical model.

[1] Both authors contributed equally to this work.

[2] To whom correspondence should be addressed. Tel./Fax: 44-1865-272451; E-mail: richard.vaughan-jones@dpag.ox.ac.uk.

[3] The abbreviations used are: CA, carbonic anhydrase; DOG, 2-deoxy-D-glucose; FS, fluorescein 5(6)-sulfonic acid; DF, *N*-(fluorescein 5-thiocarbamoyl)-1,2-dihexadecanoyl-*sn*-glycero-3-phosphoethanolamine; AP105, 1-([4-sulfamoylphenyl)ethyl]-2,4,6-trimethyl pyridinium perchlorate; ATZ, acetazolamide; EV, empty vector; ROI, region of interest; AMC, 7-amino-4-methylcoumarin; FCCP, carbonyl cyanide *p*-trifluoromethoxyphenylhydrazone; MCT, monocarboxylic acid transporter; Mes, 4-morpholineethanesulfonic acid; DIDS, 4,4′-diisothiocyanostilbene-2,2′-disulfonic acid.

perfusion), when the excreted acid/base load is elevated, or when the local buffering capacity is compromised.

Regulation of pH_e is particularly important in tumors because these are characterized by a high metabolic rate (16, 17) and abnormal blood perfusion (18, 19). Studies have shown that tumors develop low pH_e (~6.9) in response to the mismatch between metabolic demand and the capacity to remove metabolic waste products (14, 18, 20). Tumors can survive in considerably more acidic interstitium than their non-neoplastic counterparts, partly because of their ability to maintain a favorably alkaline pH_i for growth and development (21). It has been argued that tumors can survive selectively by maintaining a level of pH_e that is lethal to normal cells but not sufficiently acidic to kill the tumor itself (2, 14, 22).

A major fraction of cell-derived acid is excreted in the form of CO_2, generated directly from the Krebs cycle or from titration of intracellular H^+ with HCO_3^-. To maintain a steep outward gradient for CO_2 excretion, extracellular CO_2 must not accumulate. This can be achieved by venting CO_2 to the nearest capillary or by reacting CO_2 locally to produce H^+ and HCO_3^-. The balance between these two fluxes is set by the diffusion distance and CO_2 hydration kinetics, respectively. Diffusion is anecdotally considered to be fast. However, over long distances, CO_2 diffusion may be slower than its local reactive flux. Assuming a CO_2 diffusion coefficient, D_{CO2}, of 2500 $\mu m^2/s$ and a spontaneous CO_2 hydration rate, k_f, of 0.14 s^{-1} (23), local CO_2 consumption by reaction will be faster than CO_2 diffusion over distances >190 μm ($\sqrt{(2 \times D_{CO2}/k_f)}$). The reactive flux can be augmented enzymatically by CA_e, to increase further the importance of reactive *versus* diffusive consumption of CO_2. If, for instance, hydration is catalyzed 10-fold, reactive CO_2 removal would exceed diffusive CO_2 removal over distances of >60 μm.

The remainder of transmembrane acid efflux takes the form of lactic acid, generated from anaerobic respiration or aerobic glycolysis (Warburg effect) (16). Lactic acid efflux can be accelerated if its extracellular concentration is kept low by diffusive dissipation or by CA_e-catalyzed extracellular titration of H^+ with HCO_3^-. It is important to note that CA_e-catalyzed hydration of extracellular CO_2 will reduce pH_e, whereas titration of extracellular lactic acid by HCO_3^- (to form CO_2, a weaker acid) will *raise* pH_e. Therefore, the capacity of CA_e to regulate pH_e will depend on the chemistry of the excreted acid. In most healthy tissues at rest, the majority of cellular acid is emitted as CO_2. Recent work on tumors also suggests a dominance of CO_2 over lactic acid (22, 24).

The role for CA_e in facilitating CO_2 removal has been demonstrated for CA4 in skeletal muscle (25) and proposed for CA9 in tumors (2, 26). Furthermore, CA9 expression is strongly up-regulated in hypoxia (5), providing a mechanism by which CA9 levels are linked to diffusion distance. A consequence of facilitated CO_2 removal is the attainment of a more uniformly alkaline pH_i across the tissue. We demonstrated this recently in three-dimensional *in vitro* tissue models imaged for pH_i (23). One prediction from that study is that CA9, although reducing pH_i nonuniformity, will give rise to local extracellular acidity, particularly at the core of multicellular growths.

If pH_e is indeed acidified by CA9, the enzyme expression may be doubly beneficial for CO_2-excreting tumors: it will help to attain (i) a favorable alkaline pH_i for growth and (ii) an acidic pH_e to facilitate invasiveness. Clinically, CA9 may serve as a target for drugs. In the present work, we image pH_e using a novel, membrane-impermeant fluorescent pH dye in multicellular spheroid growths (~35,000 cells) derived from the colon carcinoma cell line HCT116. We demonstrate a key role for CA9 in regulating both pH_i and pH_e. Furthermore, we show that, even in the hypoxic core of spheroids, the principal substrate for CA9 is cell-excreted CO_2 and that the precise effect of CA9 on pH_e depends on the relative efflux from cells of lactic acid *versus* CO_2.

MATERIALS AND METHODS

Solutions—The culture medium was Dulbecco's modified Eagle's medium containing 11 mM D-glucose or 2-deoxy-D-glucose (DOG) or D-galactose, buffered by 20 mM Hepes or 5% CO_2, 22 mM HCO_3^-. The superfusate was normal Tyrode solutions containing 4.5 mM KCl, 1 mM $CaCl_2$, 1 mM $MgCl_2$, 11 mM glucose (or DOG or galactose), buffered by either 5% CO_2 with 22 mM HCO_3^- (pH 7.4, 37 °C), 5% CO_2 with 14 mM HCO_3^- (pH 7.2, 37 °C), or 1% CO_2 with 2.2 mM HCO_3^- (pH 7.2, 37 °C) or a mixture of 2 mM + 2 mM, 10 mM + 10 mM, or 20 mM + 20 mM Hepes + Mes (pH 7.4, 37 °C). NaCl was added for a final osmolarity of 300 mOsm/kg. All of the superfusates were delivered at 2 ml/min and at 37 °C maintained by a feedback heater. Superfusates were changed rapidly (<5 s) using a switcher, supplied by two solutions in parallel.

pH Reporter Dyes—To measure pH_i, carboxy-SNARF-1 (23) was loaded into cells as the membrane-permeant acetoxymethyl ester (10 μM) for 10 min (single cells) or 45 min (spheroids). Excitation at 514 nm was provided by an argon laser. Fluorescence was measured at 580 and 640 nm, ratioed, and converted to pH_i using nigericin calibration (23). Although carboxy-SNARF-1 can also, in theory, be used to measure pH_e, it is prohibitively expensive for use in superfusion experiments. For this reason, we have implemented novel fluorescein-based, dual excitation pH dyes for imaging pH_e: fluorescein-5-(and-6-)-sulfonic acid (FS) and *N*-(fluorescein-5-thiocarbamoyl)-1,2-dihexadecanoyl-*sn*-glycero-3-phosphoethanolamine (DF). The dyes were obtained from Invitrogen. FS was used in aqueous solutions at 30 μM. DF is lipid-soluble and was loaded into cell membranes by exposing cells to 10 μM dye for 10min (27). The dyes were excited alternately at two wavelengths: near (450–456 nm) and far (488–490 nm) from the absorption isosbestic point (~460 nm). Fluorescence was collected >515 nm, ratioed, and calibrated with superfusates at different pH, buffered by 10 mM Hepes + 10 mM Mes.

Inhibitors—The CA_e inhibitor 1-([4-sulfamoylphenyl)ethyl]-2,4,6-trimethyl pyridinium perchlorate (AP105) was synthesized in house and validated previously for inhibition potency (1). Acetazolamide (ATZ), a membrane-permeant CA inhibitor, was obtained from Sigma.

Cells—HCT116 cells (radius 8.6 μm) were transfected with plasmid vector only (referred to as "empty vector" (or EV)) or plasmid vector with the cDNA for human CA9 (referred to as "CA9 expressor") and grown in McCoy's 5A medium (23). CA9 cDNA was a gift from Dr. J. Pastorek (Bratislava, Slovakia).

Tests for Carbonic Anhydrase Expression—Ice-cold cell suspension was homogenized 30–50 times and centrifuged at 3000 rpm for 10 min. Supernatant was microcentrifuged (Ti70 rotor; 8000 rpm, 45 min) to deposit the membrane fraction, which tested positive for Na^+/K^+ pump protein. Western blots tested for CA9 protein using mouse monoclonal M75 primary antibodies (a gift from Dr. J. Pastorek) (23). The clone with the highest CA9 expression was selected for growing CA9-positive spheroids.

Spheroid Growth—CA9 expressor and EV HCT116 cells were cultured in McCoy's 5A medium. Aggregation into spheroids (28) was initiated by plating 4×10^6 cells in 250-ml spinner flasks (Techne MCS, UK) spun at 40 rpm for 2–9 days. Unless stated otherwise, the media were buffered by 5% CO_2, 22 mM HCO_3^- (pH 7.4 at 37 °C).

Epifluorescence Measurement of pH_e—Single cells were superfused in a chamber mounted on a Nikon Diaphot inverted microscope with a ×40 oil immersion objective. Excitation light alternating every 250 ms between 450 and 490 nm was provided by a xenon lamp monochromator. Fluorescence was collected by a photomultiplier tube at >515 nm.

Confocal Imaging of pH_e and pH_i—Confocal imaging offers high spatial resolution. Single cells or spheroids were imaged in a superfusion chamber mounted on a Leica IRBE microscope with a ×10 dry objective. The system was coupled to an normal Tyrode TCS confocal system with argon visible (514-, 458-, or 488-nm) and argon UV (351-nm) lasers. For single cell experiments, the pinhole was set to 1 Airy unit, and each cell was defined as a region of interest (ROI). For spheroid experiments, the Airy diameter in μm was set to 15% of spheroid diameter, a compromise between adequate confocality and good photon capture. The fluorescence images were used to identify the equatorial plane of the spheroid and to produce a spheroid outline. This outline was used to generate 10 concentric, nonoverlapping layered ROIs of width equal to a tenth of spheroid radius. ROI1 was defined as the ROI at the core, and ROI10 was defined as the peripheral ROI.

Statistics—The data are presented as the means ± S.E. and tested for statistical differences with *t* test (significant differences for $p < 0.05$).

RESULTS

Characterization of Fluorescein-based Dyes—Fluorescein derivatives FS and DF were characterized for their fluorescent properties. Cell-free, 30 μM solutions of FS at different pH were studied in the confocal system under argon laser excitation, alternating between 458 and 488 nm every 4 s. To characterize DF, the cells were preloaded with dye at 10 μM for 10 min, and then dye-tagged cells were superfused with dye-free solutions at different pH under xenon lamp excitation, alternating between 450 and 490 nm every 0.25 s. Fig. 1*A* shows FS and DF emission at different pH. Fluorescence excited at the lower wavelength was less pH-sensitive, as it is nearer to the isosbestic point. The fluorescence excited at the two wavelengths was ratioed and plotted as a function of pH_e in Fig. 1*B*. The p*K* values for FS and DF were estimated to be 6.4 and 7.6 (corrected for the ratio of maximum-to-minimum fluorescence at the lower wavelength, which offsets empirically estimated affinity (29)).

For a dye to report only pH_e, it must not permeate cell membranes. The membrane permeability of FS was measured in EV cells, superfused with 30 μM dye, and imaged confocally. 45 min of exposure to FS increased cellular fluorescence by <3%, suggesting low membrane permeability (Fig. 1*C*). To determine whether DF inserts at the inner or outer leaflet of the membrane, DF-loaded cells were superfused with solutions that altered pH_e alone (changing superfusate pH_e) or pH_i alone (superfusing with ammonium or acetate salts at constant pH_e). DF fluorescence was only responsive to the former maneuver, indicating outer leaflet insertion.

We also tested whether the dyes inhibit CA activity. A 10 nM solution of bovine red cell CA2, buffered by 20 mM Hepes, was tested for CA activity (23). 0.5 ml of 100% CO_2-saturated water was injected rapidly to 1.5 ml of enzyme suspension in a stirred chamber at 4 °C. Medium pH time courses were fitted with kinetic equations for CO_2 hydration. The protocol was repeated in the presence of 30 μM FS and 100 μM ATZ. Catalysis by CA was inhibited by ATZ but unaffected by FS (Fig. 1*D*) or DF (not shown).

Measuring CA9 Activity in Single Cells—Single HCT116 cells, transfected with vector alone, or vector with the CA9 gene, were assayed for CA_e activity using the epifluorescence set-up. The cells were loaded with DF to report surface membrane pH_e (Fig. 2, *A* and *B*) (27) and superfused with solutions buffered by 1% CO_2, 2.2 mM HCO_3^- (pH 7.2). Superfusates of low buffering capacity optimized the amplitude of surface pH_e changes. The superfusate was switched rapidly to one containing 30 mM ammonium (pH 7.2) for a period of 30 s. Exposure to an equilibrated solution of NH_4^+/NH_3 drives rapid entry of NH_3 into cells. Surface pH_e is reduced as extracellular NH_4^+ deprotonates to replenish NH_3 that has entered the cell. After ~20 s, surface pH_e re-equilibrates to 7.2. On subsequent removal of the extracellular weak base, NH_3 is driven rapidly out of the cell, protonates at the outer cell surface, and transiently raises surface pH_e. Because CO_2/HCO_3^- buffer contributes to the release and consumption of H^+ ions at the cell surface, the time courses of recorded pH_e transients depend on CO_2/HCO_3^- buffer kinetics, *i.e.* CA_e activity.

Fig. 2*A* (*panel i*) shows surface pH_e transients measured in CA9-expressing cells in the absence and presence of the CA_e inhibitor, AP105 (500 nM). Expression of CA9 protein in the membrane fraction was confirmed by Western blotting. The pH_e transients were smaller and briefer in the absence of AP105. This was more evident in the alkaline direction; the area under the pH_e transient was 57% larger in the presence of inhibitor. The smaller size of pH_e transients recorded in the absence of drug is indicative of CA_e activity. The same experimental protocol was performed on EV cells that lack CA9 protein in the membrane. In this case, the pH_e transients (Fig. 2*A*, *panel ii*) were not affected by AP105, indicating the absence of CA_e activity.

To confirm the membrane impermeability of AP105 (and hence selectivity for CA_e isoforms), we tested the inhibitory potency of AP105 (500 nM) on intracellular CA activity in EV cells and compared this with the potency of ATZ (100 μM), a

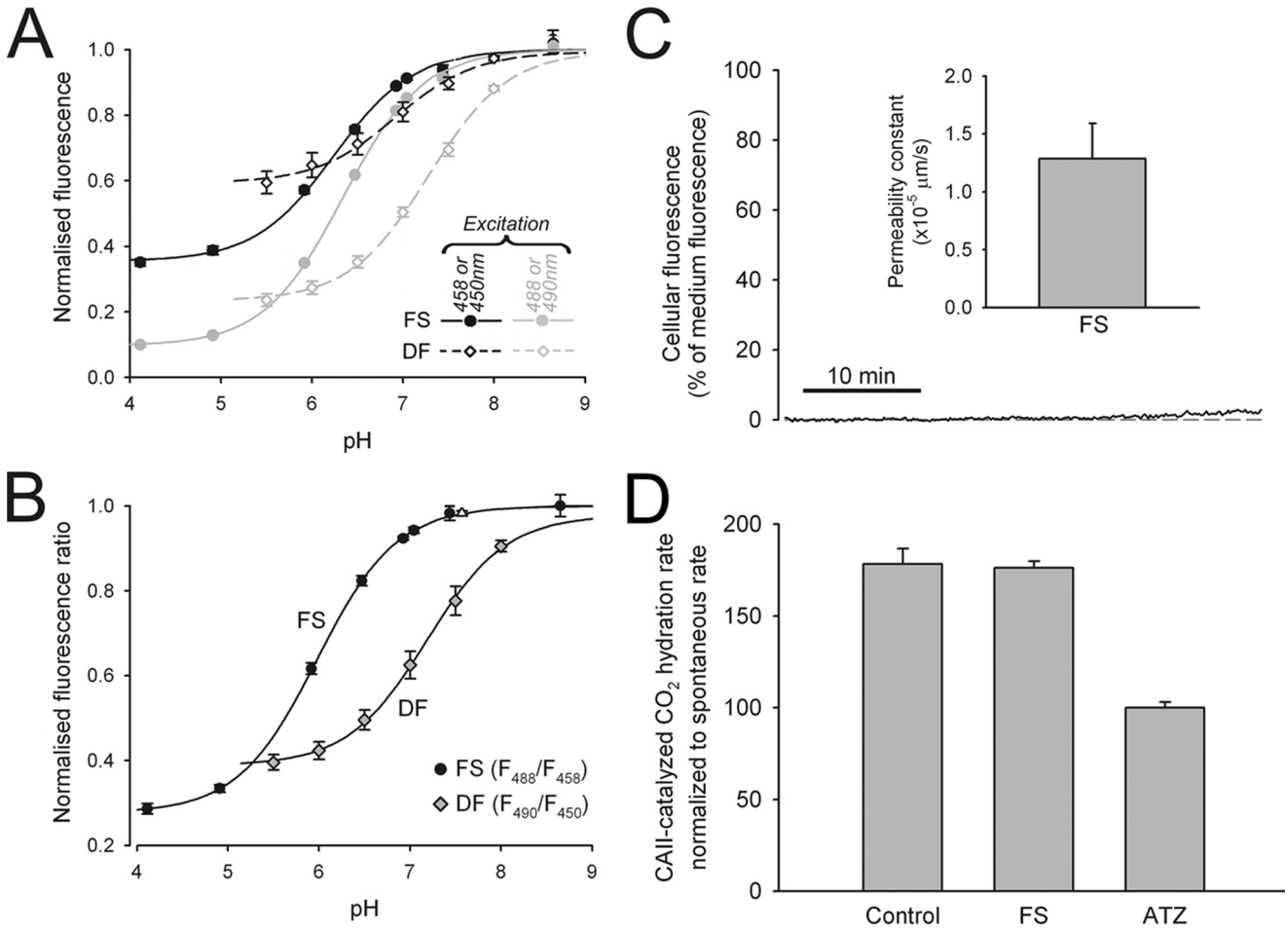

FIGURE 1. **Characterizing fluorescein-derived dyes.** *A*, fluorescence from 30 μM FS (*circles*) or from cell membranes loaded with 10 μM DF (*diamonds*), plotted *versus* superfusate pH. FS was excited at 458 nm (*black*) or 488 nm (*gray*) with an argon laser; DF was excited at 450 nm (*black*) or 490 nm (*gray*) with a xenon lamp. Data (n = 6–12/bin) were fitted to sigmoid curves. *B*, FS and DF fluorescence ratio *versus* pH. *C*, intracellular fluorescence during superfusion of EV cells with 30 μM FS, relative to superfusate fluorescence. Cellular dye uptake is negligible, indicative of low FS membrane permeability. *D*, rate of CO_2 hydration at 4 °C in the presence of 10 nM bovine red cell CA2. The rates were also measured in the presence of 100 μM ATZ or FS (n = 5/bin). The data were normalized to the ATZ (spontaneous) rate. FS does not inhibit CA2 activity.

membrane-permeant CA_e inhibitor. EV cells were loaded with the pH_i reporter dye carboxy-SNARF-1 (Fig. 2*B*) and superfused with dye-free solution. The superfusate was switched from one buffered by 20 mM Hepes (nominally CO_2-free) to one buffered by 5% CO_2, 22 mM HCO_3^-. Rapid solution change from 0 to 5% CO_2 drives CO_2 influx, intracellular hydration, and pH_i acidification. The reverse solution change produces the opposite response (23). Fig. 2*B* shows the pH_i time course associated with these maneuvers. ATZ slowed the rate of pH_i change, in both directions, but AP105 had no significant effect. The difference in response to the two drugs confirms that AP105 does not penetrate the cell membrane.

The pH_i time courses are in agreement with high membrane CO_2 permeability (estimated to be $\geq$10 μm/s). The rate of pH_i change upon the addition or removal of CO_2 provides a measure of intracellular CO_2/HCO_3^- buffering kinetics. Fig. 2*C* plots the initial rates of these pH_i changes, normalized to the rate measured in ATZ. Catalysis by intracellular CA (CA_i) isoforms alone (CA_e blocked with AP105) is 4.0- and 3.4-fold in EV and CA9-expressing cells, respectively, *i.e.* slightly greater in EV cells. This finding is consistent with the inverse relationship between CA9 and CA_i expression observed previously in RT112 cells (23). Additional CA_e activity in drug-free CA9-expressing cells augmented (by 15%) the kinetics of pH_i change on removal of extracellular CO_2, but not on its addition. CA9 has an asymmetric effect on CO_2 hydration and HCO_3^- dehydration, because the spontaneous rate of the former is slower, making it more responsive to CA9 catalysis. The pH_i time courses can also be used to derive intrinsic (non-CO_2) buffering capacity (β_i), which is given by the change in $[HCO_3^-]_i$ (which is equal to $[HCO_3^-]_o \times 10^{pH_i - pH_o}$ divided by the pH_i change (23)). β_i was 27.3 $\pm$ 0.2 and 23.5 $\pm$ 0.2 mM/pH (n = 30) in CA9-expressing and EV cells, respectively (Fig. 2*B*).

In summary, cells transfected with CA9 were positive for CA9 protein and displayed functional CA_e activity. EV cells did not express CA9 protein and showed no CA_e activity but a modestly higher CA_i activity than CA9-expressing cells.

Optical Measurements in Spheroids—The geometry of spheroids was characterized by confocal imaging with the membrane-permeant dye, 7-amino-4-methylcoumarin (AMC) (supplemental Fig. S1). Superfusion of spheroids with 10 μM AMC increased fluorescence throughout the spheroid, with an effective AMC mobility of 212 $\pm$ 12 μm^2/s, ~5-fold lower than that predicted from its molecular weight. This reduction sug-

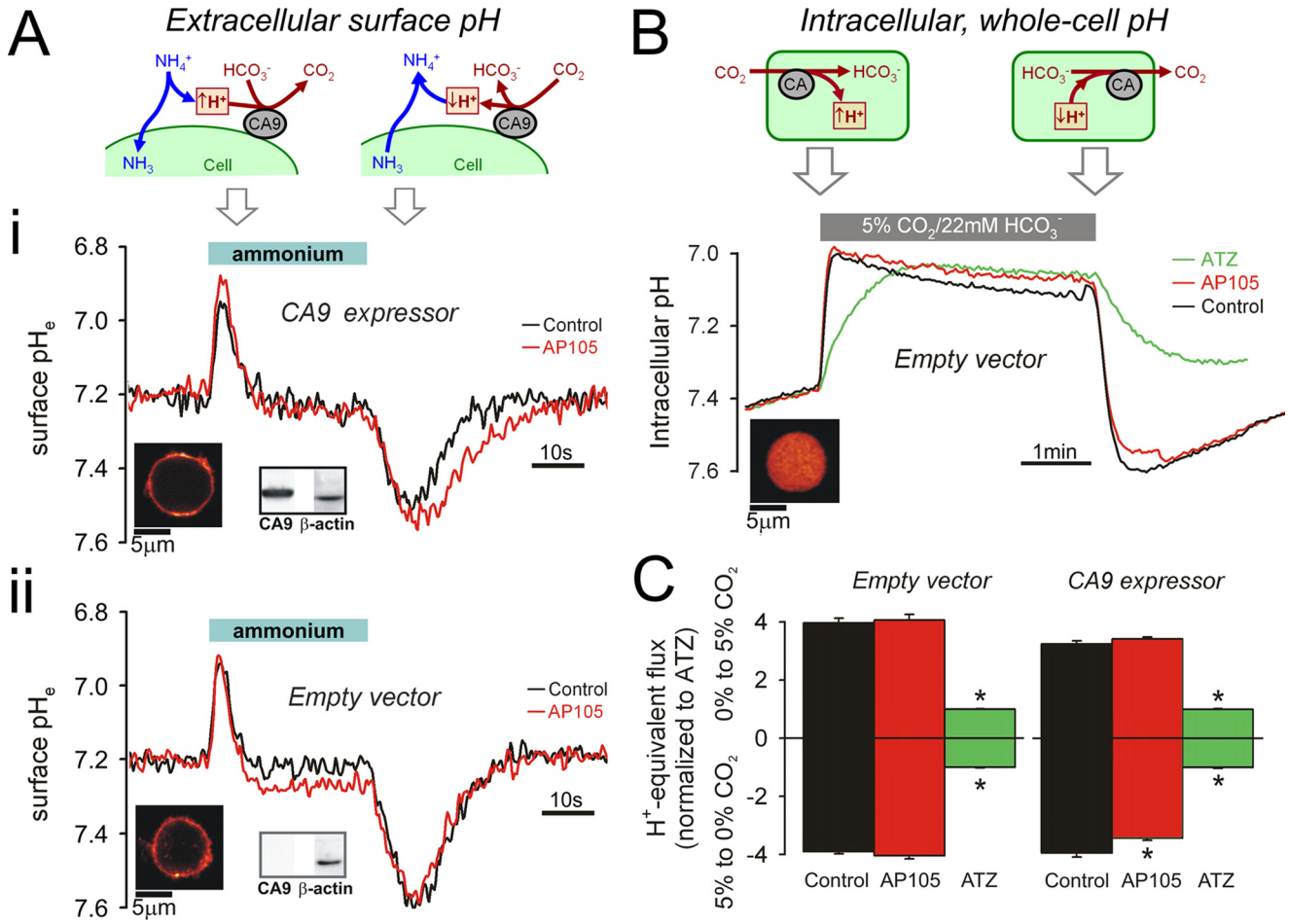

FIGURE 2. **Measuring CA activity in intact HCT116 cells.** *A*, *panel i*, CA9-expressing cells loaded with membrane-inserting dye DF (see fluorescence map). Membrane fraction tested positive for CA9 protein by Western blotting (β-actin as control). Intact cells were superfused with 1% CO_2, 2.2 mM HCO_3^- buffer (pH 7.2). Superfusion was switched rapidly for 30s to buffer containing 30 mM NH_4Cl (pH 7.2). Transmembrane NH_3 flux produces transient changes to surface membrane pH_e (*see cartoon*). Surface pH_e transients were smaller and briefer in the absence of CA9 inhibitor, 500 nM AP105 (*red*). *Panel ii*, protocol repeated on EV cells. Surface pH_e transients are not different in the presence or absence of AP105, indicating a lack of CA_e activity. *B*, EV cells AM-loaded with carboxy-SNARF-1 to measure pH_i (see fluorescence map). The cells were superfused with CO_2-free solution buffered by 20 mM Hepes (pH 7.4) and exposed for 4min to superfusate buffered by 5% CO_2, 22 mM HCO_3^- (pH 7.4). Transmembrane CO_2 flux produces pH_i changes, at a rate determined by CA catalysis (see cartoon). Protocol was repeated in the presence of AP105 (500 nM) or ATZ (100 μM). ATZ blocks all CA activity. In EV cells, AP105 has no effect on catalysis, indicating that the drug does not enter cells. *C*, initial pH_i slope on the addition and removal of CO_2 for EV ($n = 30$) and CA9 expressor cells ($n = 30$). AP105 had a small but significant effect only in CA9-expressing cells, in response to extracellular CO_2 removal.

gests that the fraction of spheroid volume occupied by cells is 80%. The restricted extracellular space is suitable for driving CO_2/HCO_3^- buffer out-of-equilibrium, a condition that allows CA_e isoforms to perform net catalysis. Steady state AMC fluorescence throughout the spheroid indicated a high degree of spherical symmetry (supplemental Fig. S1).

CA9 Enzymatic Activity Reduces Intracellular pH Gradients but Increases Extracellular pH Gradients—An earlier work (23) has shown that CA9 catalytic activity raises pH_i and reduces its spatial heterogeneity in RT112 spheroids. This observation was tested in HCT116 spheroids (radius of 150–200 μm), loaded intracellularly with carboxy-SNARF-1. The experiment could not be performed on larger spheroids because of poor dye penetrability. Steady state fluorescence was converted to pH_i maps (Fig. 3*A*) for an EV spheroid (*panel i*), a CA9-expressing spheroid under control conditions (*panel ii*), and one pretreated with 500 nM AP105 (*panel iii*). With CA9 activity, pH_i was more alkaline and spatially nearly uniform. In the absence of CA9 activity, large spatial pH_i gradients were evident, with significant acidity in core regions. Radial pH_i data are summarized in Fig. 3*C* (*panel i*).

In separate experiments, we imaged pH_e to test the hypothesis that the effect of CA9 activity on pH_e is opposite to that on pH_i (23). Spheroids (radius of 250–350 μm) were superfused with 30 μM FS solution buffered by 5% CO_2, 22 mM HCO_3^- and imaged confocally. The dye penetrates the extracellular space of the spheroid within 2 min (supplemental Fig. S2). Fig. 3*B* shows pH_e maps at steady state for an EV spheroid (*panel i*), a CA9-expressing spheroid (*panel ii*), and one pretreated with 500 nM AP105 (*panel iii*). Core pH_e was ~6.9 in the absence of CA9 (Fig. 3*B*, *panel i*) and considerably more acidic (~6.6) in its presence (Fig. 3*B*, *panel ii*). Preincubation with 500 nM AP105 for 2 h raised core pH_e to ~6.9. Radial pH_e data are summarized in Fig. 3*C* (*panel ii*). The lower pH_e measured in CA9-expressing spheroids was not due to a higher cellular metabolic rate, because both EV and CA9-expressing single cells acidified culture medium to a similar extent (supplemental Fig. S3).

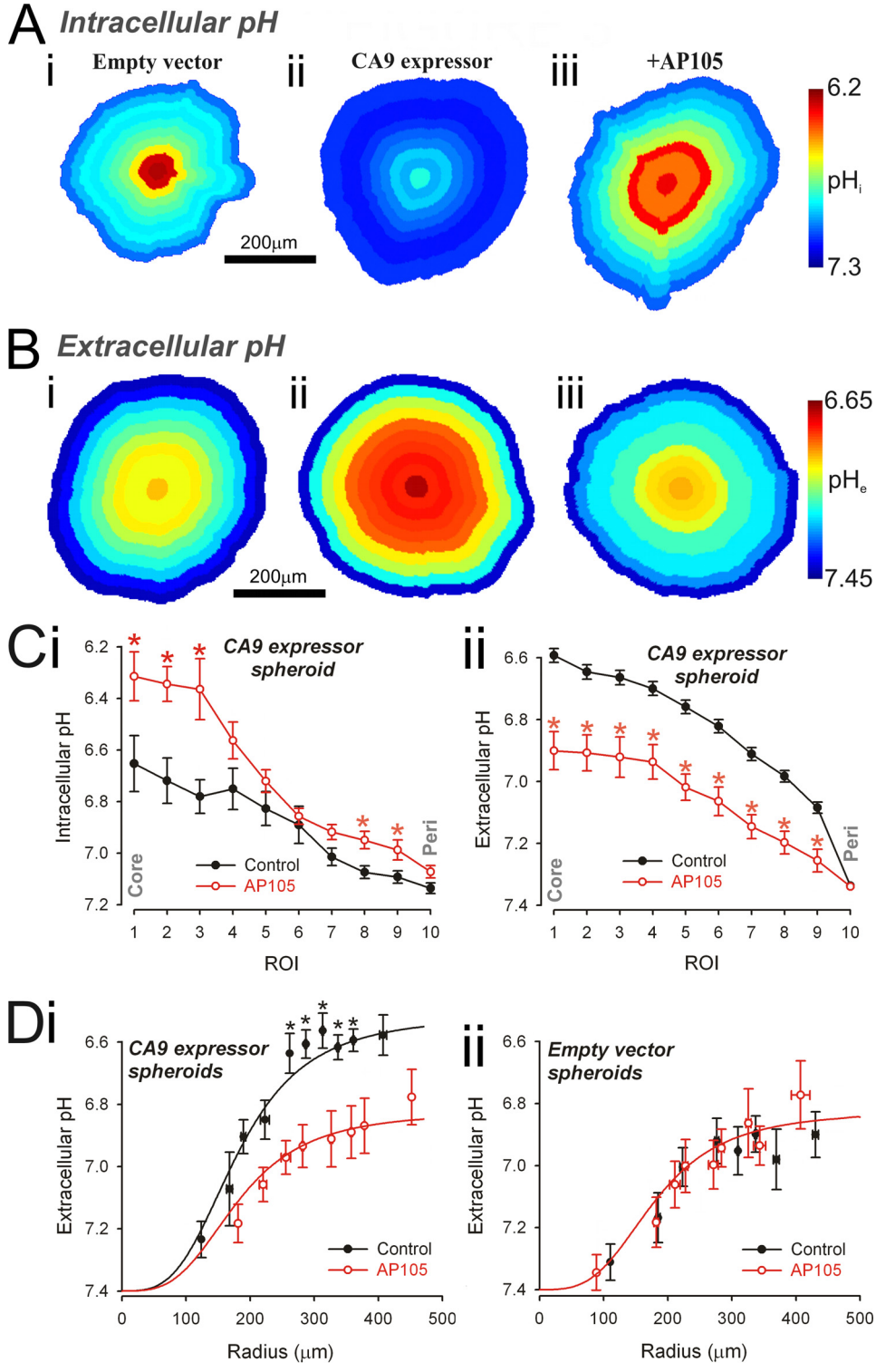

FIGURE 3. **Extracellular CA activity acidifies spheroid extracellular space and alkalinizes spheroid intracellular space.** *A* and *B*, maps of pH_i (*A*) (measured with carboxy-SNARF-1) and pH_e (*B*) (measured with fluorescein-5-(and-6-)-sulfonic acid) in EV spheroid (*panel i*), CA9-expressing spheroid (*panel ii*), and CA9-expressing spheroid preincubated with 500 nM AP105 (*panel iii*). *C*, radial profile of pH_i (*panel i*) and pH_e (*panel ii*) recorded in CA9-expressing spheroids (*black*; $n = 20$; spheroid radius of 222.0 ± 10.6 μm (*panel i*) or of 299.0 ± 2.7 μm) (*panel ii*) and in CA9-expressing spheroids treated with 500 nM AP105 (*red*; $n = 20$; spheroid radius of 229.2 ± 13.7 μm (*panel i*) or of 307.0 ± 6.3 μm) (*panel ii*). *, significant difference between control and AP105. CA9 activity decreases pH_e and increases pH_i. *D*, core pH_e measured in the presence (*red*; $n = 6–25$/bin) or absence (*black*; $n = 7–30$/bin) of AP105 in CA9-expressing spheroids (*panel i*) and EV spheroids (*panel ii*). As spheroid size increases, core pH_e decreases. The difference between CA9-expressing and EV spheroids is abolished in the presence of AP105 (best fit with three-parameter sigmoid curve).

In summary, spheroids expressing CA9 developed intracellular and extracellular acidosis that was greatest at the core. Inhibition of CA9 with AP105 reduced the radial pH_e gradient (Fig. 3*B*) but increased the radial pH_i gradient (Fig. 3*C*). The data suggest that CA9 catalytic activity accelerates the efflux of cell-derived acid to the extracellular space and helps to maintain a more uniform pH_i at the cost of a more acidic and heterogeneous pH_e.

Larger CA9-expressing Spheroids Deposit Greater Extracellular Acid Load—Acid generated by respiring cells is deposited into the extracellular space, whence it diffuses to the superfusate. The diffusion distance will determine the pace at which acid can be vented. Spheroids made from CA9 expressor or EV cells were grown to radii between 100 and 500 μm, and pH_e in the core ROI was measured in the presence and absence of 500 nM AP105 (Fig. 3*D*). In both types of spheroid, core pH_e acidified in a saturating manner as spheroid size increased. Core pH_e was 54% more acidic in CA9 expressors. Preincubation with AP105 for 2 h alkalinized core pH_e in CA9-expressing spheroids but had no effect on EV spheroids (Fig. 3*D*). These data suggest that AP105-sensitive extracellular acidity is due to CA_e activity, present in CA9-expressing spheroids but absent in EV spheroids.

Extracellular, Not Intracellular, CA Isoforms Play a Dominant Role in Acidifying pH_e—We have investigated whether inhibition of *intracellular* CA isoforms has a supplementary effect on pH_e gradients. This was examined by comparing pH_e data from spheroids (radius, 250–350 μm) preincubated with membrane-impermeant AP105 (500 nM) and membrane-permeant ATZ (100 μM). AP105 and ATZ reduced pH_e gradients by similar amounts in CA9-expressing spheroids (Fig. 4*A*, *panel i*) but had no significant effect on EV spheroids (Fig. 4*A*, *panel ii*). This indicates that, in the absence of CA_e activity, CA_i isoforms do not affect spatial pH_e gradients.

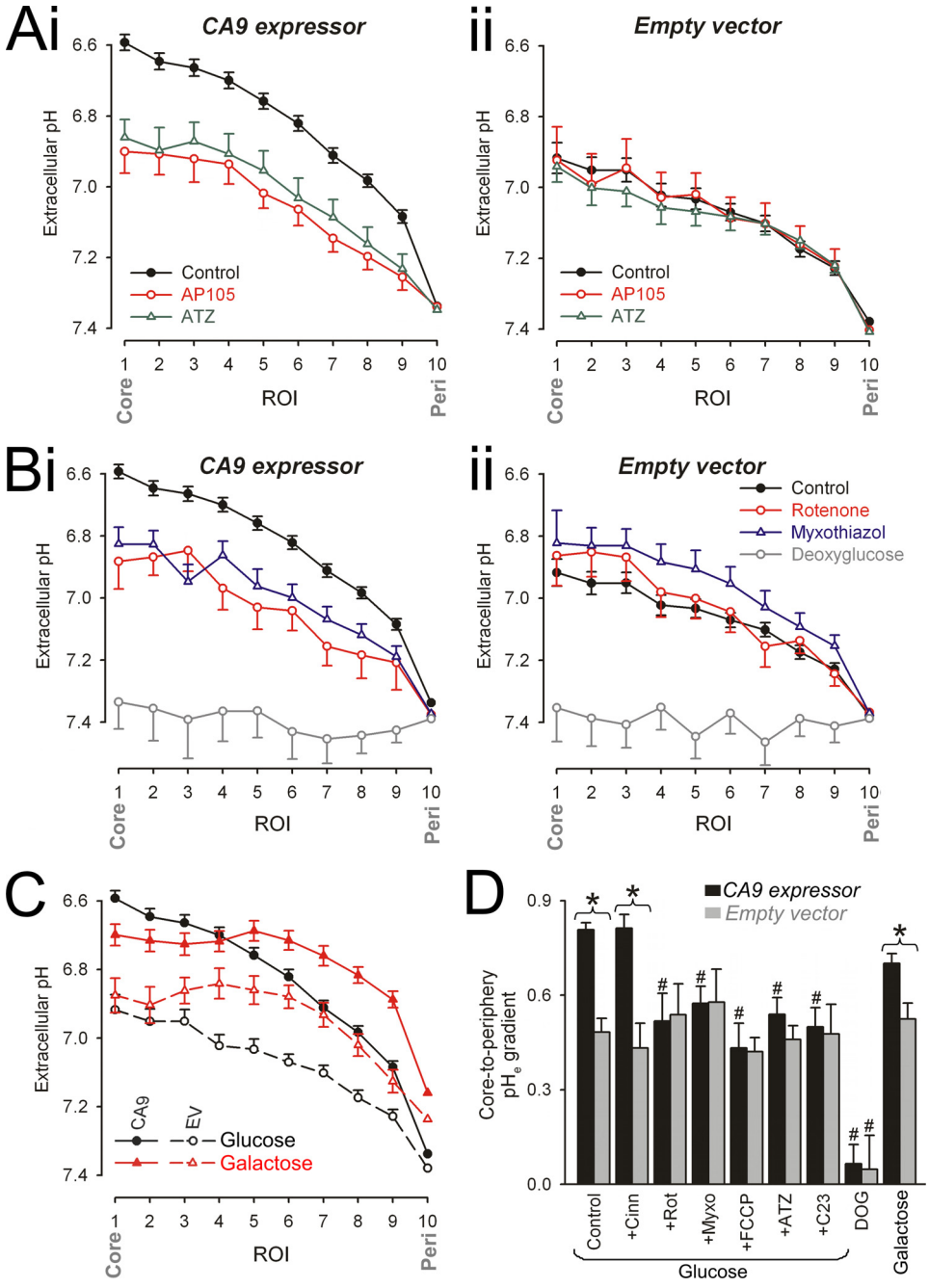

FIGURE 4. **Pharmacological studies of extracellular pH gradients.** *A–C*, imaging for pH_e with dye FS in spheroids superfused with 5% CO_2, 22 mM HCO_3^- buffer. The data are presented as radial pH_e profiles. *, significant difference between control and drug. *A*, data for CA9-expressing (*panel i*) and EV spheroids (*panel ii*). *Black filled circles*, drug-free conditions (spheroid radius of 299.0 ± 2.7 (*panel i*) and 297.6 ± 2.67 μm (*panel ii*)). *Red open circles*, with 500 nM AP105 (spheroid radius of 307.0 ± 6.3 (*panel i*) and 303.0 ± 5.7 μm (*panel ii*)); *Green open triangles*, with 100 μM ATZ (spheroid radius of 308.6 ± 3.6 (*panel i*) and 296.6 ± 6.4 μm (*panel ii*)). *B*, data for CA9-expressing (*panel i*) and EV spheroids (*panel ii*). *Black filled circles*, drug-free conditions. *Red open circles*, with 1 μM rotenone (spheroid radius of 310.0 ± 5.9 (*panel i*) and 314.7 ± 6.2 μm (*panel ii*)). *Blue open triangles*, with 5 μM myxothiazole (spheroid radius of 325.1 ± 7.2 (*panel i*) and 319.5 ± 4.2 μm (*panel ii*)). *Gray open squares*, D-glucose replaced with DOG (spheroid radius of 278.7 ± 3.6 (*panel i*) and 305.0 ± 6.6 μm (*panel ii*)). *C*, pH_e gradients in CA9-expressing spheroids (*filled symbols*) or EV spheroids (*open symbols*) respiring glucose (*black symbols*) or galactose (*red symbols*; spheroid radius of 299.4 ± 6.1 (*panel i*) and 29.5 ± 4.3 μm (*panel ii*)). *D*, core-to-periphery pH_e gradient under different conditions. *, significant difference between CA9-expressing and EV spheroids. #, significant difference between data from the same spheroid type (EV or CA9 expressor). *Cinn*, α-cyanohydroxycinnamate.

Principal Source of Substrate for Extracellular Acidification Is CO_2 Production—In experiments described thus far, glucose was the sole superfused metabolic substrate. It is thus likely to underpin the appearance of extracellular acid. To test this, spheroids (radius of 250–350 μm) were equilibrated in medium containing DOG in place of glucose to block glycolysis (30). Spheroids were subsequently superfused in DOG-containing, 5% CO_2, 22 mM HCO_3^--buffered medium and imaged for pH_e. The spheroids did not acidify pH_e (Fig. 4*B*), confirming that substrate metabolism is ultimately the source of extracellular acid.

Cells can generate acid metabolically in the form of CO_2 or lactic acid (2, 16, 17). One major source of CO_2 is decarboxylation of Krebs cycle intermediates under aerobic conditions. To investigate whether the Krebs cycle contributes to extracellular acidification, spheroids (radius 250–350 μm) were incubated for 2 h in glucose-containing medium with 1 μM rotenone or 5 μM myxothiazol, inhibitors of mitochondrial complexes I and III, respectively (31) (Fig. 4*B*). CA9-expressing spheroids, when forced to respire without Krebs cycle activity, still generated acidic pH_e gradients, but these gradients were up to 40% smaller, and were no longer significantly different from those measured in EV spheroids, *i.e.* CA_e activity under these conditions had no apparent effect on pH_e. Uncoupling of mitochondria with FCCP (25 μM) (31) had a similar effect to rotenone and myxothiazol (Fig. 4*D*). The applied doses of mitochondrial drugs were higher than typically used in isolated cells, to ensure adequate inhibition throughout the large, restricted spheroid volume. Mitochondrial inhibitors did not target *in vitro* CA9 activity (supplemental Fig. S4). In isolated cells, rotenone and myxothiazol did not have a significant effect on resting pH_i, but FCCP produced a small, transient acidification (supplemental Fig. S4).

In a different set of experiments, spheroids were grown in medium containing galactose instead of glucose. Oxidation of galactose to pyruvate yields no ATP and forces cells to commit to the Krebs cycle (32). Radial pH_e profiles were measured in CA9-expressing and EV spheroids (Fig. 4*C*). When tracking in from the

oxygenated periphery, galactose-respiring spheroids displayed a steeper fall of pH_e, in agreement with a higher Krebs cycle turnover under these metabolic conditions (32). The degree of extracellular acidosis saturated toward the core, suggesting a fall in metabolic activity in the deeper, more hypoxic regions. CA9 activity thus acidified pH_e, as expected from a CO_2-generating process.

Our data indicate that the Krebs cycle normally operates in spheroids as large as 300 μm in radius, and its output underlies much of the difference in pH_e gradients observed in CA9-expressing spheroids and EV spheroids. Fig. 4*D* summarizes the effects of different incubation conditions on the amplitude of radial pH_e gradients.

Majority of Cell Acid Is Excreted across Membranes as CO_2 Not Lactic Acid—Spheroids larger than 150 μm in radius are known to develop hypoxic cores (33, 34). Low O_2 levels activate hypoxia-inducible factor and up-regulate the anaerobic respiration of glucose to lactic acid (35). Lactic acid production is also raised when mitochondria are blocked pharmacologically. In the absence of the Krebs cycle, lactic acid production would appear to underlie much of the acidic pH_e in spheroids (Fig. 4*B*). Lactic acid production in hypoxic regions may explain why pH_e continues to fall with increasing depth in glucose-respiring spheroids but levels off in galactose-respiring spheroids (Fig. 4*C*).

Cells can remove lactic acid in two ways. The first is by intracellular titration with HCO_3^- (sequestered from the extracellular space). The titration reaction generates CO_2, which diffuses to the extracellular space, where it is subject to catalysis by CA9, if active. The second way is by extruding lactic acid directly via the monocarboxylic acid transporter (MCT) (36). Alternatively, the H^+ ion component of lactic acid can be extruded by transporters such as Na^+-H^+ exchange (9). In HCT116 cells, however, H^+ extrusion by Na^+-H^+ exchange is low and ~4-fold smaller than acid-neutralizing HCO_3^- uptake transport (supplemental Fig. S4). A similar observation has been made in RT112 cells (23). Functional MCT activity in HCT116 cells was demonstrated by measuring pH_i in isolated cells during transient exposure to 5 mM sodium lactate to activate lactic acid influx via MCT (supplemental Fig. S4). The MCT blocker α-cyanohydroxycinnamate (2.5 mM) (36) inhibited a large fraction of the acidification induced by this procedure, indicating that direct lactic acid transport is mainly MCT-mediated (supplemental Fig. S4). The contribution of MCT-mediated lactic acid excretion to pH_e nonuniformity was studied in glucose-respiring spheroids, preincubated with 2.5 mM α-cyanohydroxycinnamate for 2 h. This compound did not significantly affect pH_e gradients in either CA9 expressor or EV spheroids (Fig. 4*D*). Transmembrane lactic acid efflux therefore does not contribute greatly toward acidic pH_e under control conditions. It is therefore likely that the majority of anaerobically produced acid exits cells as CO_2, formed by titration with intracellular HCO_3^-.

Extracellular Acidification Can Be Altered by Extracellular [HCO_3^-] and Buffering Capacity—The extracellular buffering regime has a 2-fold effect on pH_e gradients. First, the magnitude of pH_e changes in response to acid depends inversely on extracellular buffering capacity. Second, extracellular CO_2/HCO_3^- buffer provides substrate (HCO_3^-) for cellular uptake and titration with intracellular acid. To investigate the effect of extracellular buffering capacity and composition, the spheroids were preincubated for 6 h under one of two conditions. In one set of experiments, incubation and subsequent superfusion was performed in lower extracellular [HCO_3^-] (5% CO_2, 14 mM HCO_3^-, pH 7.2). Radial pH_e profiles were measured in CA9-expressing spheroids. Compared with experiments in 22 mM HCO_3^- media, acidic pH_e gradients were greater in low HCO_3^- medium, in agreement with its lower buffering capacity. Inhibition of CA9 with AP105 had a similar effect on pH_e gradients under both buffering conditions (Fig. 5*A*).

In a second set of experiments, spheroids were preincubated and then superfused with Hepes and Mes buffer (2 + 2 mM, 10 + 10 mM, or 20 + 20 mM) in place of CO_2/HCO_3^-. An equimolar mixture of Hepes + Mes ensures that buffering capacity is near constant over the pH_e range 6–7.5. Overall, increasing the extracellular buffering capacity in CA9-expressing or EV spheroids decreased pH_e gradients (Fig. 5, *B–D*). Spheroids expressing CA9 activity produced larger pH_e gradients than EV spheroids (Fig. 5, *B* and *D*). Preincubation with 500 nM AP105 reduced pH_e gradients in CA9-expressing spheroids to levels observed in EV spheroids (Fig. 5*C*). The relationship between pH_e gradient size and Hepes + Mes buffering (Fig. 5*E*) indicates that extracellular buffering by 5% CO_2, 22 mM HCO_3^- corresponds to an equivalent Hepes + Mes concentration of ~17 mM.

In summary, our data show that CA9 can acidify pH_e even in the absence of superfusate CO_2/HCO_3^- buffer. This confirms that the principal source of extracellular acid is cell-derived CO_2, much of this being generated from the Krebs cycle.

DISCUSSION

Carbonic Anhydrase 9 as a Regulator of Both Intracellular and Extracellular pH—The extracellular topology of the CA9 active site has hinted at a role in acidifying pH_e. Expression of the enzyme in a population of isolated cells reduces medium pH (26). In single cells, expression of CA9 has been shown to raise steady state pH_i (3), and our previous work (23) has shown that CA9 activity raises pH_i and reduces its heterogeneity in multicellular spheroid growths. All of these results suggest that CA9, in effect, increases the transmembrane acid efflux.

In the present work, we have tested this hypothesis by *in vitro* imaging of both pH_i and pH_e in spheroids grown from cells of the HCT116 human colon carcinoma line. This cell line has a high metabolic rate (supplemental Fig. S3) and can grow into multicellular spheroids that are accessible to confocal imaging (Fig. 3 and supplemental Figs. S1 and S2). Spheroids are a good model for poorly perfused, developing tumors (23, 28, 33) because they have a restricted extracellular space, with a considerable core-to-surface diffusion distance for solutes such as CO_2 and H^+ ions. Spheroids may also offer a useful experimental model for simulating pH control during interrupted vascular perfusion of normal tissue, such as brain and myocardium. We have characterized a novel dye, fluorescein-5-(and-6)-sulfonic acid, and we find that it provides excellent spatial measurements of pH_e in spheroids. Under control conditions, spheroids develop radial gradients of pH_i and pH_e, with the lowest levels

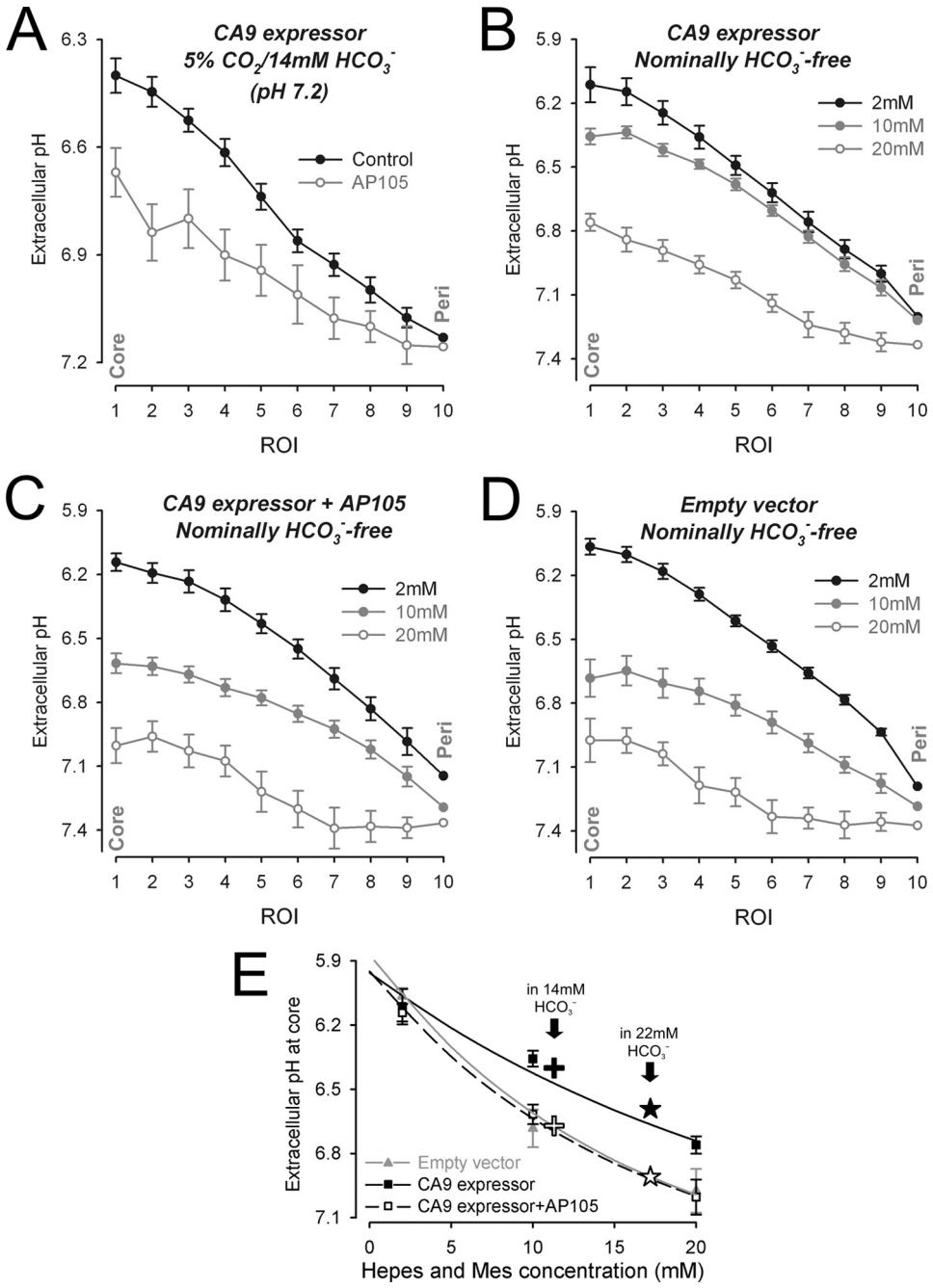

FIGURE 5. **Extracellular pH gradients in low or nominally nil HCO_3^- superfusates.** Spheroids were equilibrated in media buffered by 5% CO_2/14 mM HCO_3^- (pH 7.2) (*A*) or an equimolar mixture (2 + 2, 10 + 10, 20 + 20 mM) of Hepes + Mes buffer (pH 7.4) instead of CO_2/HCO_3^- (*B–D*). Radial pH_e profiles (n = 10–22/data set) in CA9-expressing spheroids with and without 500 nM AP105 (*A*; radius of 377.6 ± 6.2 and 362.6 ± 6.6 μm), CA9-expressing spheroids (*B*; radius of 274.3 ± 5.7, 285.3 ± 13.8, and 285.0 ± 7.2 μm), CA9-expressing spheroids preincubated with 500 nM AP105 (*C*; radius of 271.3 ± 7.3, 272.6 ± 4.5, and 277.6 ± 6.9 μm), and EV spheroids (*D*; radius of 280.9 ± 7.0, 261.9 ± 4.1, and 263.3 ± 6.2 μm). *E*, core-to-periphery pH_e gradient *versus* Hepes + Mes concentration. *Stars* and *crosses*, superimposition of pH_e gradient measured in 5% CO_2, 22 mM HCO_3^- buffer and 5%CO_2, 14 mM HCO_3^- buffer with (*black filled symbols*) or without (*open symbols*) CA9 activity.

reached at the core (Fig. 3*C*). Expression of CA9 decreases core pH_e and increases core pH_i (Fig. 3, *A–C*), supporting a role for CA9 in facilitating transmembrane acid efflux.

Sources of Extracellular Acidosis and the Role of CA9—We studied the factors, including CA9 activity, that affect pH_e. The degree of extracellular acidity increases with spheroid radius (Fig. 3*D*), as expected from the increasing diffusion distance. The ultimate source of acid in the extracellular space is cellular respiration, because removal of metabolizable substrate causes spheroid pH_e to equilibrate with the superfusate (Fig. 4*B*). There are three possible ways for cells to generate extracellular acid (Fig. 6*A*): (i) J_{mito}, mitochondrial CO_2 production and its efflux; (ii) J_{extr}, lactic acid production and H^+-lactate extrusion by MCT or H^+ ion extrusion by *e.g.* Na^+-H^+ exchange, and (iii) J_{titr}, lactic acid production, its titration by intracellular HCO_3^- and subsequent efflux in the form of CO_2. In general, these acid fluxes will occur in all tissues, but the distribution among the three pathways will depend on factors such as oxygenation, mitochondrial status, membrane transporter activity, and the chemistry of the respiratory substrate. For example, removing extracellular HCO_3^-, by eliminating HCO_3^- reuptake into cells, will reduce J_{titr} to 0 but increase J_{extr}, to ensure sustained removal of lactic acid. Another example is that substituting glucose with galactose forces cells to rely entirely on oxidative phosphorylation rather than anaerobic respiration (32). Under these conditions, J_{titr} and J_{extr} will fall to 0, whereas J_{mito} and O_2 consumption will rise.

Intracellular and extracellular CA isoforms could potentially play a role in all three acid efflux pathways (Fig. 6*A*). Our data, however, show that inhibition of CA_i isoforms has no supplementary effect on pH_e gradients when CA9 activity is absent, indicating that the major influence of CA on pH_e is exerted through CA_e (Fig. 4*A*). CA9 activity accelerates both extracellular CO_2 hydration and the reverse dehydration reaction. If cellular acid is excreted as CO_2, CA9 will increase its extracellular hydration, yielding more H^+ (thus lowering pH_e), thereby facilitating further transmembrane CO_2 efflux. If cellular acid is excreted as lactic acid, CA9 will facilitate its extracellular titration with HCO_3^-. This will augment transmembrane lactic acid efflux but will *increase* pH_e. This is because CO_2 is a weaker and more diffusible acid than lactic acid. Therefore, CA9 will have opposing effects on pH_e, depending on whether CO_2 or lactic acid are principally extruded. Either way, CA9 will facilitate the

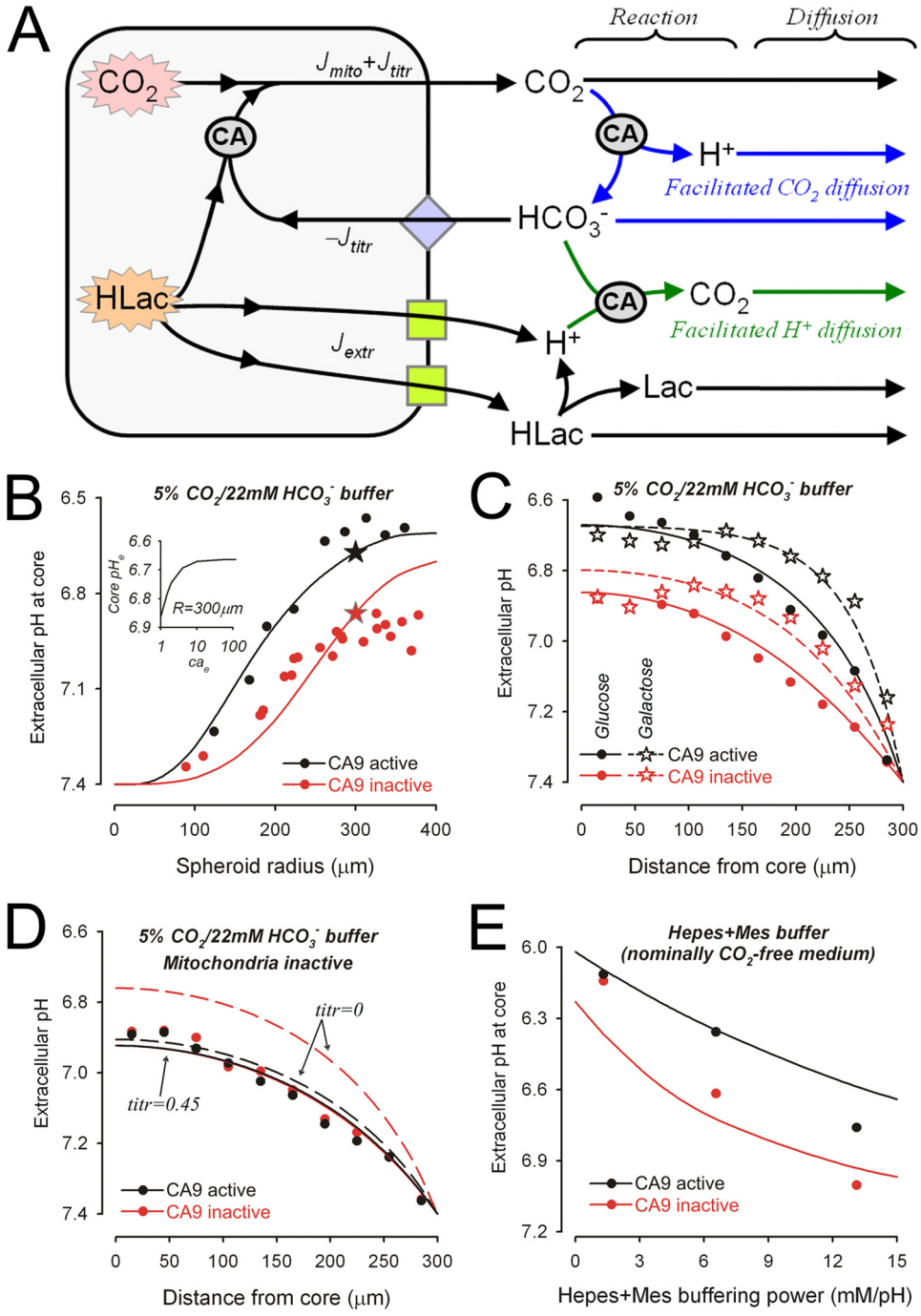

FIGURE 6. **Model of spheroid pH_e regulation.** *A*, proposed scheme of acid efflux pathways. Cell metabolism generates acid which takes the form of CO_2 or lactic acid (*HLac*). CO_2 generated directly by mitochondria (J_{mito}) can exit across the membrane. The acidity caused by lactic acid can be extruded across the membrane as H^+ ions (J_{extr}) by H^+-lactate co-transport or H^+ extrusion (*green squares*). Alternatively lactic acid can be titrated with intracellular HCO_3^-, imported on transmembrane HCO_3^- carriers (*blue diamond*), to produce CO_2 (J_{titr}). Extracellular pH depends on acid output and the extracellular diffusion and reaction fluxes. Carbonic anhydrases (*circled CA*) catalyze the reaction $CO_2 + H_2O \leftrightarrow H^+ + HCO_3^-$. *B*, experimental data (from Fig. 3*D*) with model simulation for the relationship between core pH_e and spheroid radius in 5% CO_2, 22 mM HCO_3^- buffer. To obtain the sigmoidal relationship, F_{subs} μM/s) is 180−(0.3 × radius). *Red*, CA inactive (CA_e = 1); *black*, CA active (CA_e = 10); *stars*, core pH_e for radius = 300 μm. *Inset*, relationship between core pH_e and CA activity (CA_e). *C*, experimental data (from Figs. 4, *A* and *C*) with model simulation for radial pH_e gradients in glucose-respiring (*circles*) or galactose-respiring (*stars*) spheroids in 5% CO_2, 22 mM HCO_3^- buffer. *D*, experimental data (from Fig. 4*B*) with model simulation (*continuous line*) for radial pH_e gradients in 5% CO_2, 22 mM HCO_3^- buffer in the presence of mitochondrial inhibitors. The fraction of intracellular lactic acid titrated was 0.45. *Dashed line*, model simulation assuming nil intracellular lactic acid titration. *E*, experimental data (from Fig. 5) with model simulation for core pH_e at increasing Hepes + Mes buffer capacity.

efflux of acid (CO_2 or lactic acid). The fact that, in control spheroids CA9 acidifies pH_e indicates that its principal effect is to facilitate the efflux of cellular CO_2. In support of this model, radial pH_e gradients were not significantly affected by blocking MCT (Fig. 4*D*). Furthermore, the activity of other H^+ ion extruding transporters (*e.g.* Na^+-H^+ exchange) in HCT116 cells is low (supplemental Fig. S4), and so their contribution to H^+ efflux will be minimal. This is in agreement with data from *in situ* colon carcinomas, showing that ~70% of acid output is as CO_2 (22, 24).

In well oxygenated regions of spheroids, most CO_2 will originate from the Krebs cycle (J_{mito}). Indeed, in galactose-respiring spheroids, this is the only source of cellular acid. It is therefore notable that radial pH_e profiles in these spheroids were steep near the periphery but leveled off sharply with depth, in contrast to a smoother and more gradual pH_e acidification toward the core of glucose-respiring spheroids (Fig. 4*C*). The steepness of the radial pH_e gradient at the periphery of galactose-respiring spheroids can be explained by a high respiration rate in these regions, as observed previously in cultured cells (32). The flatter pH_e gradient at depths >170 μm indicates a sharp drop in acid production, correlating with the predicted fall in O_2 tension. In contrast, pH_e continues to fall with depth in glucose-respiring spheroids, suggesting a sustained acid production that persists under hypoxia.

As O_2 tension falls, lactic acid production will increase. Because CA9 has an acidifying effect on pH_e, even at the hypoxic core of spheroids (Fig. 3*C*, *panel ii*), it is likely that cell-generated lactic acid in these regions is titrated (J_{titr}) with HCO_3^- to produce CO_2, which then vents from cells to act as a substrate for CA_e. For this process to be maintained, HCO_3^- must be continuously transported back into the cell from the extracellular space. The role of HCO_3^- influx transporters in

determining J_{titr} could be studied with pharmacological inhibitors. However, many inhibitors of acid/base transport, such as DIDS, also inhibit CA activity directly (37); therefore it was not feasible to use these drugs in our studies of CA9. However, the role that J_{titr} plays in providing substrate (CO_2) for CA9 can be appreciated by removing extracellular HCO_3^-, thus blocking HCO_3^- re-uptake (Fig. 5). Over a comparable pH_e range, the acidifying effect of CA9 on pH_e was 15% smaller in spheroids superfused in Hepes/Mes buffer than in 5% CO_2, 22 mM HCO_3^- buffer (Fig. 5*E*).

In the presence of mitochondrial inhibitors, spheroids continued to produce an acidic pH_e, but there was now no observable influence of CA9 activity (Fig. 4*B*). Under these conditions, J_{mito} is abolished, and all acid efflux is carried by $J_{extr} + J_{titr}$. The lack of effect of CA9 under these conditions argues for a balance between J_{extr} and J_{titr}, at which there is no net CA9 catalysis, *i.e.* catalyzed CO_2 hydration (driven by J_{titr}) and its catalyzed reverse reaction (driven by J_{extr}) cancel out.

Mathematical Model of the Role of CA9—To understand the complex acid/base events occurring in spheroids, it was necessary to construct a quantitative diffusion reaction model (see supplemental material for details). By fitting experimental data to the model, we were able to estimate J_{mito}, J_{extr}, and J_{titr}, as well as extracellular buffering capacity (β_e), extracellular H^+ mobility (D_e), and CA_e activity (CA_e). These parameters could not be derived directly from any one set of data, because they require a unifying mathematical framework to fit several data sets simultaneously. The very good fits to experimental data (Fig. 6, *B–E*) further support the conclusions made above.

Total acid production depends on the rate of metabolic substrate respiration (F_{subs}). The model predicts $F_{subs} = 90$ μM/s in glucose-respiring spheroids (radius, 300 μm). This rate is in agreement with measurements of 30–190 μM/s, previously made in spheroids (34). But glucose consumption rates in tumors have been reported to be an order of magnitude lower than this (2–15 μM/s) (18). These latter data, however, may have been underestimated F_{subs} values, because they were normalized to total tumor mass, including its blood supply, stroma, and dead cells, which do not contribute to tumor cell F_{subs}.

In control spheroids, the local O_2 tension determines whether metabolic substrate is respired aerobically to CO_2 (J_{mito}) or anaerobically to lactic acid ($J_{titr} + J_{extr}$). Our model predicts that the rate of aerobic respiration decays exponentially toward the spheroid core, with a space constant of 250 μm. This is in agreement with radial O_2 measurements in spheroids (33, 34) that fit to an exponential decay, with depth (x), $\exp(-x/\lambda_{O_2})$, giving a space constant (λ_{O_2}) of 150–650 μm. For galactose-respiring spheroids, the model predicts that F_{subs} is raised 4-fold, and λ_{O_2} is reduced to 45 μm, in agreement with the higher oxidative phosphorylation rate measured in cultured cells (32).

Lactic acid production shows an opposite depth dependence, $1-\exp(-x/\lambda_{O_2})$, *i.e.* it increases with depth, unless the metabolic substrate is galactose, which is not respired anaerobically. A certain fraction of lactic acid is titrated by intracellular HCO_3^- (J_{titr}), and the remainder is extruded by H^+ transporters (J_{extr}). The relationship between J_{titr} and J_{extr} can be estimated by best fitting the model to experimental data. Under control conditions (Fig. 6, *B* and *C*), a large fraction of lactic acid is predicted to undergo intracellular titration. In nominally HCO_3^--free superfusate (Fig. 6*E*), all lactic acid is predicted to be extruded directly.

Under control conditions, the lowering of pH_e by CA9 activity is consistent with a 10-fold catalysis of CO_2 hydration ($CA_e = 10$; Fig. 6*B*). However, in spheroids with drug-inhibited mitochondria ($J_{mito} = 0$), CA9 activity had no apparent effect on pH_e gradients. This is expected to occur at a certain balance between J_{titr} and J_{extr}, because these acid fluxes drive the CA9-assisted reaction in opposite directions. Using the model it is possible to calculate that this balance is attained when 45% of lactic acid is titrated intracellularly (Fig. 6*D*).

Our data cannot provide independent estimates for β_e and D_e, but best fitting their product, $D_e \times \beta_e$, yields a value of 1.6×10^4 mM·μm²/s. This implies that as β_e increases, D_e must decrease, in agreement with the finding that H^+ buffers lower the effective H^+ ion mobility (38).

Conditions for CA9 Catalysis—Using our experimental data and computational modeling, we can now define the conditions under which CA9 catalysis exerts a significant effect on pH_e. Condition 1: Cells must engage in metabolic acid production (Fig. 4*B*). Our results suggest that the ability of CA9 to decrease pH_e increases with respiration rate (F_{subs}). In the presence of galactose, the elevated F_{subs} increases the steepness of radial pH_e profiles within the aerobic zone (Fig. 6*C*). Condition 2: The effect of CA9 on pH_e will depend on the type of acid released across the cell membrane. Our model predicts that the greatest acidifying effect of CA9 on pH_e is observed if all substrate is respired aerobically to CO_2 (Fig. 6*C*). The greatest alkalinizing effect of CA9 on pH_e will be observed if all glucose is respired to lactic acid, without any titration by HCO_3^- (*dashed curves* in Fig. 6*D*). The observation that, *in vivo*, pH_e is low in most cancers (14, 18, 20) suggests that CO_2 excretion is important in CA9-expressing tumors, such as colon cancer (2, 22, 24), and that efflux of lactic acid may be dominant in tumors lacking CA_e activity, such as gastric cancer (39). This may define different phenotypes of cancer pH_e, with implications for the selection of therapies that target their metabolism. Condition 3: Cellular uptake of HCO_3^- can drive extracellular CO_2/HCO_3^- buffer out-of-equilibrium and allow CA9 to exert a net catalytic effect, particularly when HCO_3^- influx is combined with CO_2 efflux (*i.e.* counter flux). This arrangement between CA and an acid/base transporter has been called a HCO_3^- transport metabolon (40, 41). Condition 4: The buffering properties of the extracellular space will affect the equilibrium between H^+, CO_2, and HCO_3^-. If, in our model, D_e and/or β_e are increased, then the predicted pH_e gradients become smaller. When $[H^+]_e$ is "buffered" by raised $D_e \times \beta_e$, CO_2/HCO_3^- buffer is more prone to be driven out-of-equilibrium by transmembrane CO_2 or HCO_3^- flux. Therefore, the effect of CA9 on pH_e gradients will be greater at higher $D_e \times \beta_e$ (Fig. 6*E*). Condition 5: The level of CA9 catalysis can vary because of spatial differences in expression. Such variations in CA9 activity may therefore affect local pH_e. CA9 expression levels in stably transfected spheroids are nearly uniform (23), but as CA9 expression is hypoxia-induced (5), the enzyme may not be uniformly distributed in poorly perfused tissues or tumors. Our computational model, how-

ever, shows that the effect of CA9 on pH_e is saturable (Fig. 6*B*, *inset*); therefore spatial variations in CA9 catalysis above ~20-fold will not affect pH_e greatly in regions where overall expression is high. In addition, the need for CA9 catalysis to maintain CO_2/HCO_3^- equilibrium is less at shorter distances from the blood supply. Therefore, CA9 activity in well oxygenated peripheral areas will be redundant, and expression levels there will not affect pH_e. This redundancy may explain the correlation between CA9 expression and hypoxia in tumors (42).

Conclusions—Carbonic anhydrases are found in virtually all cells. CA_e isoforms have generated considerable attention because of their postulated role in facilitating acid removal from cells. CA9 is of particular interest because of its association with cancer and its hypothesized role in regulating metabolism. To elucidate the physiological role for CA_e isoforms, extracellular CO_2/HCO_3^- buffer must be driven out-of-equilibrium. This will happen in the restricted extracellular environment of respiring spheroids and in poorly perfused but metabolically active tissue. CA9 activity facilitates acid removal by accelerating the conversion of excreted product (CO_2 or lactic acid) to its conjugate pair (HCO_3^- or lactate). The CA9-dependent reaction flux then becomes significant, compared with diffusive removal of waste products. Inhibition of CA9 activity impedes acid efflux and increases intracellular acidity (Fig. 3*C*, *panel i*). In well perfused tissue (including the peripheral regions of spheroids), diffusion distances are small enough to ensure rapid waste product removal, making CA9 catalysis redundant. In deeper regions, simple diffusion of acid waste products cannot be accelerated, but expression of CA_e isoforms offers a tool by which cells can engage in *facilitated* diffusion. A consequence of CA_e activity is extracellular acidification (when CO_2 is hydrated) or alkalinization (when HCO_3^- is dehydrated). Therefore, expression of CA_e isoforms is a means by which cells can modulate pH_e. Because the source of acid/base disturbance affecting pH_e is the cell, changes in pH_e will be mirrored by opposite changes in pH_i. Extracellular CA9 (and presumably other CA_e isoforms, such as CA4, CA12, and CA14) therefore acts as a "catalytic converter" for the acid exhaust system of respiring cells. Inhibition of CA9 activity in CO_2-excreting tumors may thus provide a strategy for suppressing their development, by acidifying pH_i (to attenuate growth (2, 21)) and alkalinizing pH_e (to eliminate the selective advantage of neoplastic cells (8, 22)).

Acknowledgments—We acknowledge I. Ledaki, A. Hulikova, and P. Cobden for excellent assistance in culturing spheroids.

REFERENCES

1. Supuran, C. T. (2008) *Nat. Rev. Drug Discov.* **7,** 1–14
2. Swietach, P., Vaughan-Jones, R. D., and Harris, A. L. (2007) *Cancer Metastasis Rev.* **26,** 299–310
3. Chiche, J., Ilc, K., Laferrière, J., Trottier, E., Dayan, F., Mazure, N. M., Brahimi-Horn, M. C., and Pouysségur, J. (2009) *Cancer Res.* **69,** 358–368
4. Pastorek, J., Pastoreková, S., Callebaut, I., Mornon, J. P., Zelník, V., Opavský, R., Zat'ovicová, M., Liao, S., Portetelle, D., Stanbridge, E. J., Závada, J., Burny, A., and Kettmann, R. (1994) *Oncogene* **9,** 2877–2888
5. Wykoff, C. C., Beasley, N. J., Watson, P. H., Turner, K. J., Pastorek, J., Sibtain, A., Wilson, G. D., Turley, H., Talks, K. L., Maxwell, P. H., Pugh, C. W., Ratcliffe, P. J., and Harris, A. L. (2000) *Cancer Res.* **60,** 7075–7083
6. Ludwig, M. G., Vanek, M., Guerini, D., Gasser, J. A., Jones, C. E., Junker, U., Hofstetter, H., Wolf, R. M., and Seuwen, K. (2003) *Nature* **425,** 93–98
7. Waldmann, R., Champigny, G., Lingueglia, E., De Weille, J. R., Heurteaux, C., and Lazdunski, M. (1999) *Ann. N.Y. Acad. Sci.* **868,** 67–76
8. Huang, W. C., Swietach, P., Vaughan-Jones, R. D., Ansorge, O., and Glitsch, M. D. (2008) *Curr. Biol.* **18,** 781–785
9. Boron, W. F. (2004) *Adv. Physiol. Educ.* **28,** 160–179
10. Jean, T., Frelin, C., Vigne, P., Barbry, P., and Lazdunski, M. (1985) *J. Biol. Chem.* **260,** 9678–9684
11. Stewart, A. K., Kurschat, C. K., Vaughan-Jones, R. D., and Alper, S. L. (2009) *J. Biol. Chem.* **284,** 6126–6139
12. Chambard, J. C., and Pouyssegur, J. (1986) *Exp. Cell Res.* **164,** 282–294
13. Pouysségur, J., Sardet, C., Franchi, A., L'Allemain, G., and Paris, S. (1984) *Proc. Natl. Acad. Sci. U.S.A.* **81,** 4833–4837
14. Gatenby, R. A., Gawlinski, E. T., Gmitro, A. F., Kaylor, B., and Gillies, R. J. (2006) *Cancer Res.* **66,** 5216–5223
15. Kato, Y., Nakayama, Y., Umeda, M., and Miyazaki, K. (1992) *J. Biol. Chem.* **267,** 11424–11430
16. Gatenby, R. A., and Gillies, R. J. (2004) *Nat. Rev. Cancer* **4,** 891–899
17. Gillies, R. J., Robey, I., and Gatenby, R. A. (2008) *J. Nucl. Med.* **49,** (Suppl. 2) 24S–42S
18. Vaupel, P., Kallinowski, F., and Okunieff, P. (1989) *Cancer Res.* **49,** 6449–6465
19. Stubbs, M., McSheehy, P. M., Griffiths, J. R., and Bashford, C. L. (2000) *Mol. Med. Today* **6,** 15–19
20. Gillies, R. J., Raghunand, N., Karczmar, G. S., and Bhujwalla, Z. M. (2002) *J. Magn. Reson. Imaging* **16,** 430–450
21. Griffiths, J. R., Stevens, A. N., Iles, R. A., Gordon, R. E., and Shaw, D. (1981) *Biosci. Rep.* **1,** 319–325
22. Griffiths, J. R., McIntyre, D. J., Howe, F. A., and Stubbs, M. (2001) *Novartis Found. Symp.* **240,** 46–62
23. Swietach, P., Wigfield, S., Cobden, P., Supuran, C. T., Harris, A. L., and Vaughan-Jones, R. D. (2008) *J. Biol. Chem.* **283,** 20473–20483
24. Holm, E., Hagmüller, E., Staedt, U., Schlickeiser, G., Günther, H. J., Leweling, H., Tokus, M., and Kollmar, H. B. (1995) *Cancer Res.* **55,** 1373–1378
25. Geers, C., and Gros, G. (2000) *Physiol. Rev.* **80,** 681–715
26. Svastová, E., Hulíková, A., Rafajová, M., Zat'ovicová, M., Gibadulinová, A., Casini, A., Cecchi, A., Scozzafava, A., Supuran, C. T., Pastorek, J., and Pastoreková, S. (2004) *FEBS Lett.* **577,** 439–445
27. Stock, C., Mueller, M., Kraehling, H., Mally, S., Noël, J., Eder, C., and Schwab, A. (2007) *Cell Physiol. Biochem.* **20,** 679–686
28. Sutherland, R. M. (1988) *Science* **240,** 177–184
29. Grynkiewicz, G., Poenie, M., and Tsien, R. Y. (1985) *J. Biol. Chem.* **260,** 3440–3450
30. Pelicano, H., Martin, D. S., Xu, R. H., and Huang, P. (2006) *Oncogene* **25,** 4633–4646
31. Wallace, K. B., and Starkov, A. A. (2000) *Ann. Rev. Pharmacol. Toxicol.* **40,** 353–388
32. Marroquin, L. D., Hynes, J., Dykens, J. A., Jamieson, J. D., and Will, Y. (2007) *Toxicol. Sci.* **97,** 539–547
33. Carlsson, J., and Acker, H. (1988) *Int. J. Cancer* **42,** 715–720
34. Kunz-Schughart, L. A., Doetsch, J., Mueller-Klieser, W., and Groebe, K. (2000) *Am. J. Physiol. Cell Physiol.* **278,** C765–C780
35. Semenza, G. L. (2003) *Nat. Rev. Cancer* **3,** 721–732
36. Halestrap, A. P., and Price, N. T. (1999) *Biochem. J.* **343,** 281–299
37. Villafuerte, F. C., Swietach, P., and Vaughan-Jones, R. D. (2007) *FASEB J.* **21,** A1284
38. Swietach, P., and Vaughan-Jones, R. D. (2005) *J. Physiol.* **566,** 793–806
39. Pastoreková, S., Parkkila, S., Parkkila, A. K., Opavský, R., Zelník, V., Saarnio, J., and Pastorek, J. (1997) *Gastroenterology* **112,** 398–408
40. Sterling, D., Reithmeier, R. A., and Casey, J. R. (2001) *J. Biol. Chem.* **276,** 47886–47894
41. Morgan, P. E., Pastoreková, S., Stuart-Tilley, A. K., Alper, S. L., and Casey, J. R. (2007) *Am. J. Physiol. Cell Physiol.* **293,** C738–C748
42. Airley, R. E., Loncaster, J., Raleigh, J. A., Harris, A. L., Davidson, S. E., Hunter, R. D., West, C. M., and Stratford, I. J. (2003) *Int. J. Cancer* **104,** 85–91